ANALYSIS OF A BRIDGE APPROACH: LONG-TERM BEHAVIOUR FROM SHORT-TERM RESPONSE

G. Ognibene[1*], W. Powrie[1], L. Le Pen[1] and J. Harkness[1]
The University of Southampton, Southampton, U.K.
go1n15@soton.ac.uk

ABSTRACT

Transition zones are locations where trackbed support conditions change abruptly, for example from an earth embankment onto a bridge. The track geometry at these sites degrades faster than regular railway track, requiring more frequent and costlier maintenance. To improve understanding of the underlying causes and improve maintenance and design methods, numerical studies are often carried out, although it is computationally expensive and generally not feasible to mimic a sufficient number of loading cycles to represent reality. This paper explores an approach to predicting the long term performance of a bridge approach based on a short term simulation. Three novel performance indicators are suggested, based on existing empirical settlement equations. The dynamic response of a real ballasted railway bridge transition was studied using a Finite Element (FE) model, and the effects of train speed, sub-base soil and under sleeper pads (USPs) were investigated. Results show that both the train speed and the sub-base material affect transition performance. In accordance with previous studies, a stiffer, wedge-shaped backfill was found to mitigate the adverse effects of the support stiffness variation at the bridge approach under idealised conditions. Adding USPs appeared to have a relatively minimal influence on track long term performance.

1. INTRODUCTION

Transition zones often experience higher geometry degradation rates than regular track (e.g. Briaud, James and Hoffman, 1997; ERRI, 1999; Sasaoka and Davis, 2005; Li, Otter and Carr, 2010; Mishra *et al.*, 2012). Transition zones are locations where there are abrupt changes in geometry and / or track support conditions. Typical examples include track over culverts, bridge ends, tunnel portals and level crossings. As a train travels along the track, its vertical position is affected by changes to the stiffness and damping of the track, as well as by any changes in vertical track level. This results in excitation of the vehicle mass components (bogies, car body and wheels), associated changes in their vertical accelerations, and variation of the wheel-rail contact force. The wheel load is supported through a combination of the bending stiffness of the rail and the compliant components beneath (e.g. the railpads and the trackbed), which may be considered as springs in series per sleeper. Owing to the interactive load carrying capacity provided by rail bending stiffness and the longitudinally varying trackbed spring stiffness per sleeper, the load transferred through to the trackbed may be more erratic than the wheel/rail contact force. An increased variation in the peak loads / stresses transferred to the trackbed causes more rapid differential settlement and geometry quality deterioration of the track.

At bridge approaches, initial variation in support conditions and the differing propensities to settle of the earthwork and the bridge lead to developing geometry faults with cumulative loading (Briaud, James and Hoffman, 1997; Hoppe, 1999; Seo, 2003). In previous studies, field measurements indicated differential permanent settlements of 7 mm or 10 mm after a half year of operation (Coelho, 2011), and up to 10 mm after 10 months of operation (Stark and Wilk, 2015). Field observations of four bridge transition zones in

Kansas (U.S.) showed a mean settlement on the bridge of 8 mm and the free track of 20 mm (Li and Davis, 2005). The differential settlement between the bridge deck and the earthwork leads to the development of bumps (or dips) and hanging sleepers.

Field investigations are relatively difficult to implement because monitoring usually requires access to a trafficked zone. The utility of numerical models may be limited by a lack of validation data from field studies. Numerical studies may consider short and / or long-term analyses, in which track performance (e.g. sleeper deflection, sleeper-ballast pressure) is assessed after single and / or multiple train passes. Modelling can be used to predict track settlement and to compare the relative performance of different transition designs. Ideally, long term modelling would always be implemented. Current computational techniques usually require settlement equations to relate the ballast settlement to one or more parameters such as the number of load cycles, maximum sleeper-ballast pressure (e.g. Sato, 1997) or maximum sleeper deflection (e.g. Guérin, 1996). Settlement equations can be used in iterative models where a dynamic train-track analysis is performed and an outcome is used as input to a defined settlement equation to predict the settlement of the ballast, after a certain number of further cycles, for each sleeper. The track level is then updated, and the procedure is repeated (e.g. Varandas et al., 2014; Wilk and Stark, 2016; Wang, 2018, Nielsen and Li, 2018 and Grossoni *et al.*, 2019). However, there are limitations in the empirical settlement equations currently used, which are not usually fully validated in the field and / or able to consider variations in load (Dahlberg, 2001; Abadi *et al.*, 2016).

Owing to the lack of reliable long term settlement equations, most bridge transition models have been used for short-term simulations (e.g. Gallego *et al.*, 2012, 2016; Ribeiro, 2012; Varandas, *et al.* 2014; Paixão, *et al*. 2014, 2016; Stark *et al.* 2015; Ribeiro *et al.* 2015).

This paper contributes to the modelling of bridge transitions in the short term, exploring how short term outputs might be used to predict the potential for the development of long term differential settlements. Novel performance parameters are proposed and assessed for their potential to predict the long term performance of a bridge transition without carrying out a cyclic analysis. These are based on the assumption that the differential settlement of the ballast can be predicted from initial variations in load at the sleeper-ballast interface. This is taken into account by considering two model outputs: the maximum deflection of the sleeper into the ballast and maximum sleeper-ballast contact pressure. The dynamic response of an existing bridge transition from a recently constructed bridge on the Thameslink route was studied using an FE model. The effects of train speed, different sub-base soil types and under sleeper pads (USPs) were investigated.

2. BRIDGE STUDY SITE

An existing reinforced concrete integral bridge, where the railway passes over a road (FIGURE 2.1), was used in this study. The track is ballasted, both on the approach earthworks and over the bridge. The route comprises a single line of standard gauge, with continuously welded 54 kg/m rails and 2.5 m long mono-block concrete sleepers spaced at 0.65 m. The bridge has a span of about 11.75 m, a height of approximately 5 m and width of 6.3 m. FIGURE 2.1 shows the longitudinal (x-z plane) view. The abutments of the bridge are each supported by eight reinforced concrete piles of diameter 600 mm and height 15 m, spaced 900 mm apart. The transition comprises a wedge-shaped backfill and reinforced concrete approach slab. The backfill

to the abutments has a height of about 5 m and comprises two inclined granular layers: 6N/6P and 1A (Manual of Contract Documents for Highway Works, 2016). The approach slab has a length of 8 m, and its thickness varies from 300 mm to 750 mm close to the abutment. The total length of the transition zone is about 12.2 m.

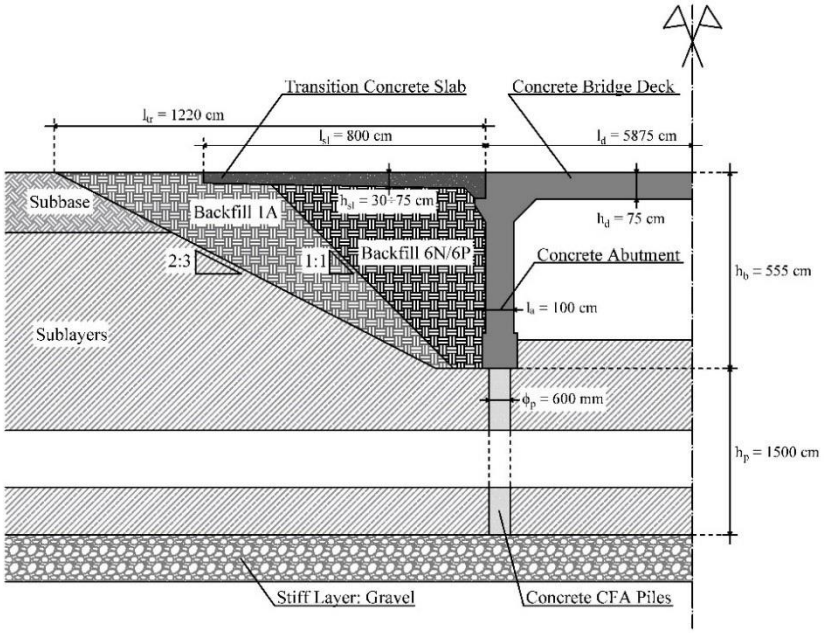

FIGURE 2.1. Longitudinal view (x-z plane) of the railway bridge transition.

3. DESCRIPTION OF THE NUMERICAL MODEL

General aspects

A 2D Finite Element (FE) model was created using the software ABAQUS. The model comprises a total length of 170.3 m (262 sleepers) and is made up of 37,000 elements (four-node plane strain elements: CPE4R) with 31,566 nodes. A schematic view is shown in FIGURE 3.1, which also indicates the layering adopted for parameterisation of the ground. The substructure is formed of 30 cm of ballast, 170 cm of sub-base and sublayers. The sublayers were divided into nine parts to facilitate a change in material properties with depth. First, to account for the increase in stiffness of soil, the Young's modulus of the sublayers was increased linearly from the top to the bottom layers. Then, to approximate 3D effects in a 2D analysis, the Young's moduli were further increased to reduce vertical strain and mimic the effect of lateral load spreading (Ribeiro, 2012). The base of the model was rigidly fixed, and the ends were free to move vertically. A full train model was used and the rail, pad and sleeper properties lumped to replicate equivalent 2D values (FIGURE 3.2). All of the railway track components were modelled using four-node plane-strain elements. Apart from the ballast and backfill materials, which were assigned Mohr-Coulomb elastic / fully plastic properties, the material behaviour was assumed to be linear-elastic. The length and depth of the model were chosen to mitigate, in combination with viscous boundary conditions (White, Lee and Valliappan (1977), the effect of wave reflections; the depth of 20 m below the sleeper base was also sufficient to reduce stresses at the bottom of the mesh to less than 10% of their values at the sleeper base. Key material properties and the corresponding source references are given in TABLE 3.2. Further details are given in Ognibene (2016). The implementation also required key interfaces / interactions to be defined as shown in TABLE 3.1.

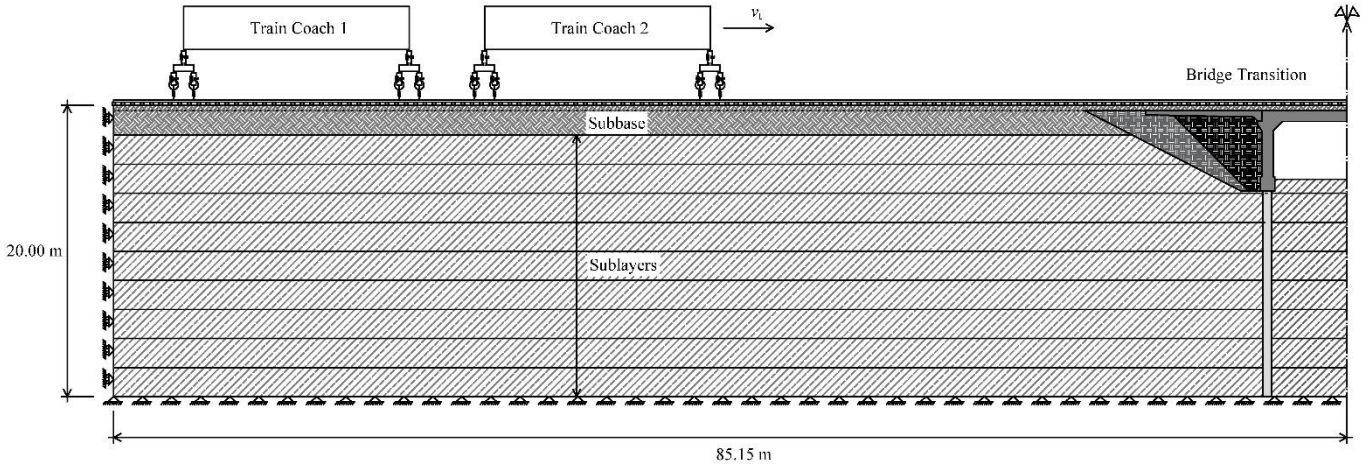

FIGURE 3.1. Longitudinal view (x-z plane) of the half of the railway track model (it is symmetric).

TABLE 3.1. Interaction properties adopted in the FE model.

Interaction	Tangential behaviour	Normal behaviour	Allowing separation?
Wheels-rail	Frictionless	Hard contact: linear penalty method	yes
Rail-railpad	-	Surface tie contact (perfectly rigid contact)	-
Railpad-sleeper	-	Surface tie contact (perfectly rigid contact)	-
Sleeper-ballast	Static-kinetic exponential decay	Hard contact: linear penalty method	no

The sublayers (FIGURE 3.1) were modelled as natural silty sand and with a stiffening soil with depth (see TABLE 3.2). In one simulation, the effect of USPs on transition response was investigated. Twenty-eight USPs were installed beneath the sleepers from the mid-span of the bridge on either side, to cover the entire transition zone (FIGURE 4.1b).

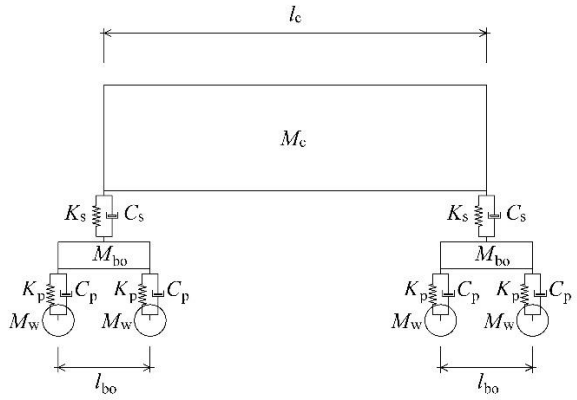

FIGURE 3.2. Geometrical representation of one train coach.

The model was initially run with a stationary train on the left-hand side and gravitational acceleration set to 9.81 m.s^{-2}. The crib ballast was not included in the model, so a load representing its weight was applied. A dynamic, implicit method (full Newton-Raphson method) was then used to solve the non-linear dynamic problem with a train velocity v_t.

TABLE 3.2. Key properties of the model.

Item	Key properties	Source
Train	M_c = 56,400 kg; M_{bo} = 4,000 kg; M_w = 1,000 kg; l_c = 22.9 m, l_{bo} = 2.6 m	Publicly available for class 221 (*Supervoyager*)
	$K_p = K_s = 2.3 \cdot 10^6$ N.m^{-1} ; $C_p = C_s = 2.0 \cdot 10^6$ N.s.m^{-1}	Assumed based on literature (e.g. Alves Ribeiro *et al.*, 2015; Arlaud *et al.*, 2016)
Rail	$E = 210 \cdot 10^9$ Pa; $\upsilon = 0.3$; $\rho = 4{,}992$ kg·m^{-3}	UIC54 rail (BS EN 13674-1)
Railpad	$E = 4.8 \cdot 10^6$ Pa; $\upsilon = 0.49$; $\rho = 1{,}000$ kg·m^{-3}	Assumed based on literature (e.g. Alves Ribeiro *et al.*, 2015; Arlaud *et al.*, 2016).
Sleeper	$E = 20 \cdot 10^9$ Pa; $\upsilon = 0.2$; $\rho = 2{,}400$ kg·m^{-3}	G44 sleeper (NR/L2/TRK/030)
Undersleeper pad	$E = 10.0 \cdot 10^6$ Pa; $\upsilon = 0.1$; $\rho = 428$ kg·m^{-3}; h = 2 mm	Sylomer® SLB 3007 G (Getzner Wekstoffe)
Approach slab	$E = 33.3 \cdot 0.6 \cdot 10^9$ Pa; $\upsilon = 0.2$; $\rho = 2{,}400$ kg·m^{-3}	EN 1991-1-1 (×0.6 for cracking)
Abutments	$E = 35.2 \cdot 0.6 \cdot 10^9$ Pa; $\upsilon = 0.2$; $\rho = 2{,}400$ kg·m^{-3}	
Deck	$E = 35.2 \cdot 0.6 \cdot 10^9$ Pa; $\upsilon = 0.2$; $\rho = 2{,}400$ kg·m^{-3}	
Piles	$E = 33.3 \cdot 0.6 \cdot 10^9$ Pa; $\upsilon = 0.2$; $\rho = 2{,}400$ kg·m^{-3}	
Backfill 1A	$E = 60 \cdot 10^6$ Pa; $\upsilon = 0.30$; $\rho = 1{,}500$ kg·m^{-3}	Manual of Contract Documents for Highway Works (2016)
Backfill 6N/6P	$E = 100 \cdot 10^6$ Pa; $\upsilon = 0.30$; $\rho = 1{,}600$ kg·m^{-3}	
Ballast	$E = 150 \cdot 10^6$ Pa; $\upsilon = 0.30$; $\rho = 1{,}650$ kg·m^{-3}	Assumed based on literature (e.g. Alves Ribeiro *et al.*, 2015; Arlaud *et al.*, 2016)
Sublayers	$E(z) = 30 \cdot 10^6 \cdot (z/d)$ Pa; $\upsilon = 0.30$; $\rho = 1{,}750$ kg·m^{-3} d is the depth at which E is known (set equal to 2 m), z is the depth starting from the sleeper base.	Natural silty sand, values based on literature (e.g. Powrie, 2013)

Sub-base properties

The sub-base (see FIGURE 3.1) is modelled with three different sets of properties to cover a range of possible soil conditions in the UK: (a) firm clay, (b) medium-dense sand, and (c) soft clay (TABLE 3.3). Soil properties were determined based on the soil description at the site, engineering judgement and relevant literature (e.g. Powrie, 2013).

TABLE 3.3. Sub-base properties adopted for the different soil types.

	E [Pa]	υ [-]	c [kPa]	φ [°]	ψ [°]	ρ [kg·m^{-3}]
Firm clay	$24 \cdot 10^6$	0.45	N/A	N/A	N/A	2,000
Medium-dense sand	$50 \cdot 10^6$	0.30	1	32	10	1,800
Soft clay	$12 \cdot 10^6$	0.45	N/A	N/A	N/A	1,900

Model calibration

Adjustments were made to the Young's moduli of the track substructure components (ballast, sub-base and sublayers) to account for 3D stress redistribution (lateral spreading). To determine the appropriate adjustments, comparisons were made with an equivalent 3D model of a short length of track loaded vertically by a single wheel load. FIGURE 3.3a presents the vertical displacements of the nodes under the applied load for the 3D and 2D models after the calibration process. The factors k_i to apply to each Young modulus are shown in FIGURE 3.3b and were obtained following an iterative method similar to the one proposed by Ribeiro (2012).

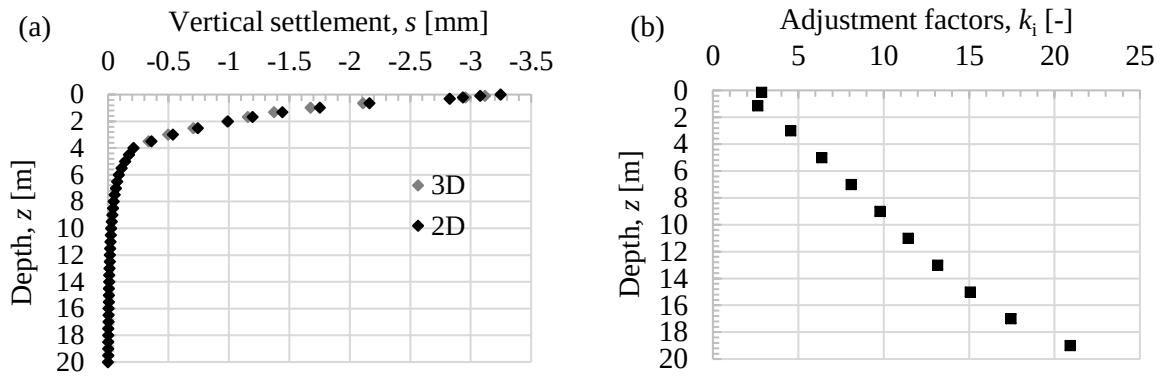

FIGURE 3.3. 2D/3D calibration of the model (a) vertical settlement under the load with depth, and (b) required 2D soil layer Young's modulus adjustment factors.

4. NUMERICAL SIMULATIONS

Parametric Study

The simulations carried are summarized in TABLE 4.1. The first part of the study investigated the behaviour of the bridge approach with and without the planned transition solution (backfill with approach slab) and the effect of adding under sleeper pads (FIGURE 4.1). The second part investigated the dynamic behaviour of the bridge approach with different sub-base materials (medium-dense sand, stiff clay, soft clay) and train speeds (30, 40, 50 m·s^{-1}).

TABLE 4.1. Summary of analyses carried out.

Part	Simulation	Train speed, v_t	Transition solution	Sub-base material
1	1	40 m·s^{-1}	None	Medium-dense sand
	2	40 m·s^{-1}	Backfill + Approach Slab	Medium-dense sand
	3	40 m·s^{-1}	Backfill + Approach Slab + USPs	Medium-dense sand
2	4	30 m·s^{-1}	Backfill + Approach Slab	Medium-dense sand
	5	30 m·s^{-1}	Backfill + Approach Slab	Firm clay
	6	30 m·s^{-1}	Backfill + Approach Slab	Soft clay
	7	50 m·s^{-1}	Backfill + Approach Slab	Medium-dense sand
	8	50 m·s^{-1}	Backfill + Approach Slab	Firm clay
	9	50 m·s^{-1}	Backfill + Approach Slab	Soft clay

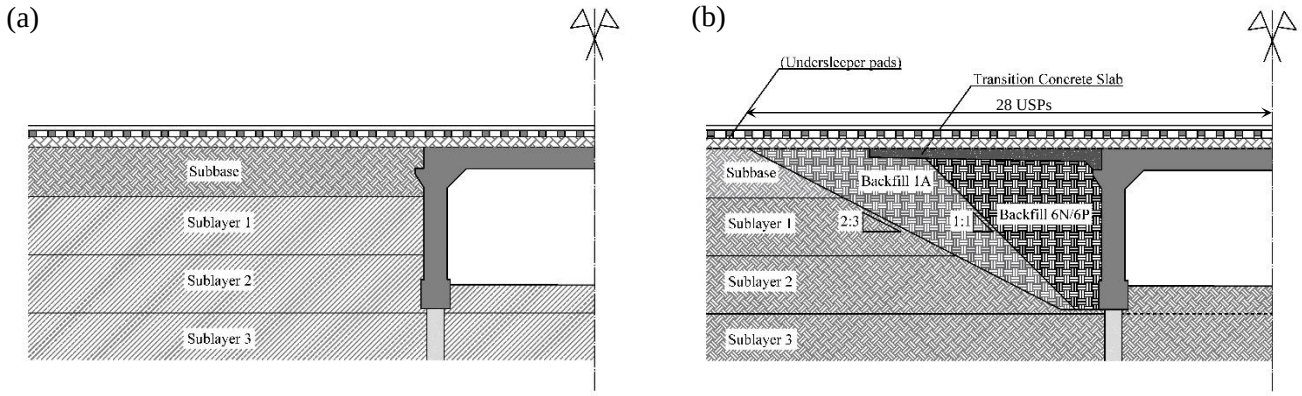

FIGURE 4.1. (a) No Solution: Simulation #1; (b) Backfill + Approach Slab (+ USPs): Simulations #2-9.

Model Initialisation

An initial permanent settlement profile was prescribed to the track (common for each simulation), varying from about 4 mm near the bridge abutment to about 8 mm on the embankment (FIGURE 4.2a). In this condition, sleepers #111 and #152 had gaps beneath them of about 0.1 mm (FIGURE 4.2b).

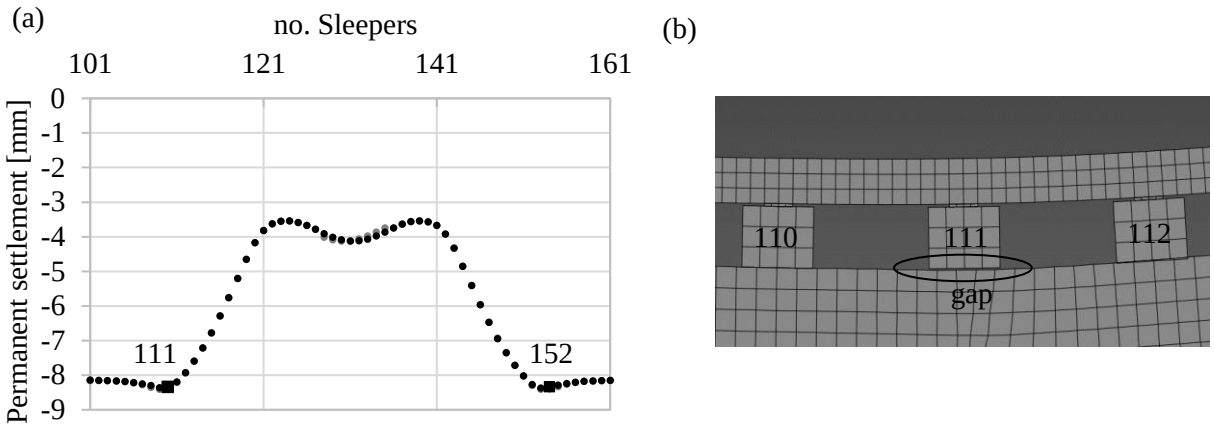

FIGURE 4.2. (a) Settlement profile along the transition zone used as an initial condition; (b) hanging sleeper (#111) resulted from the permanent differential settlement (not to scale).

5. RESULTS

The simulations have been assessed in terms of maximum ballast contact pressures and the maximum downward deflections of the sleepers (#101 to #161) on the bridge (FIGURE 5.1).

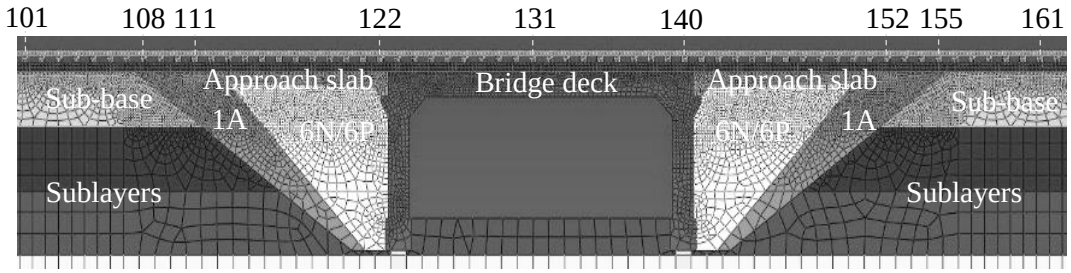

FIGURE 5.1. Section of the track of interest (from sleeper #101 to #162).

FIGURE 5.2a and 5.2c show the maximum sleeper-ballast contact pressure p_{bmax} for different train speeds (for a soft clay sub-base) and transition solutions (for a medium-dense sand sub-base), respectively. FIGURE 5.2b and 5.2d compare the result in terms of the maximum downward sleeper deflection, $u_{s,max}$.

FIGURE 5.3 shows the corresponding graphs for different sub-base materials and train speeds of 30 m·s^{-1} and 50 m·s^{-1}.

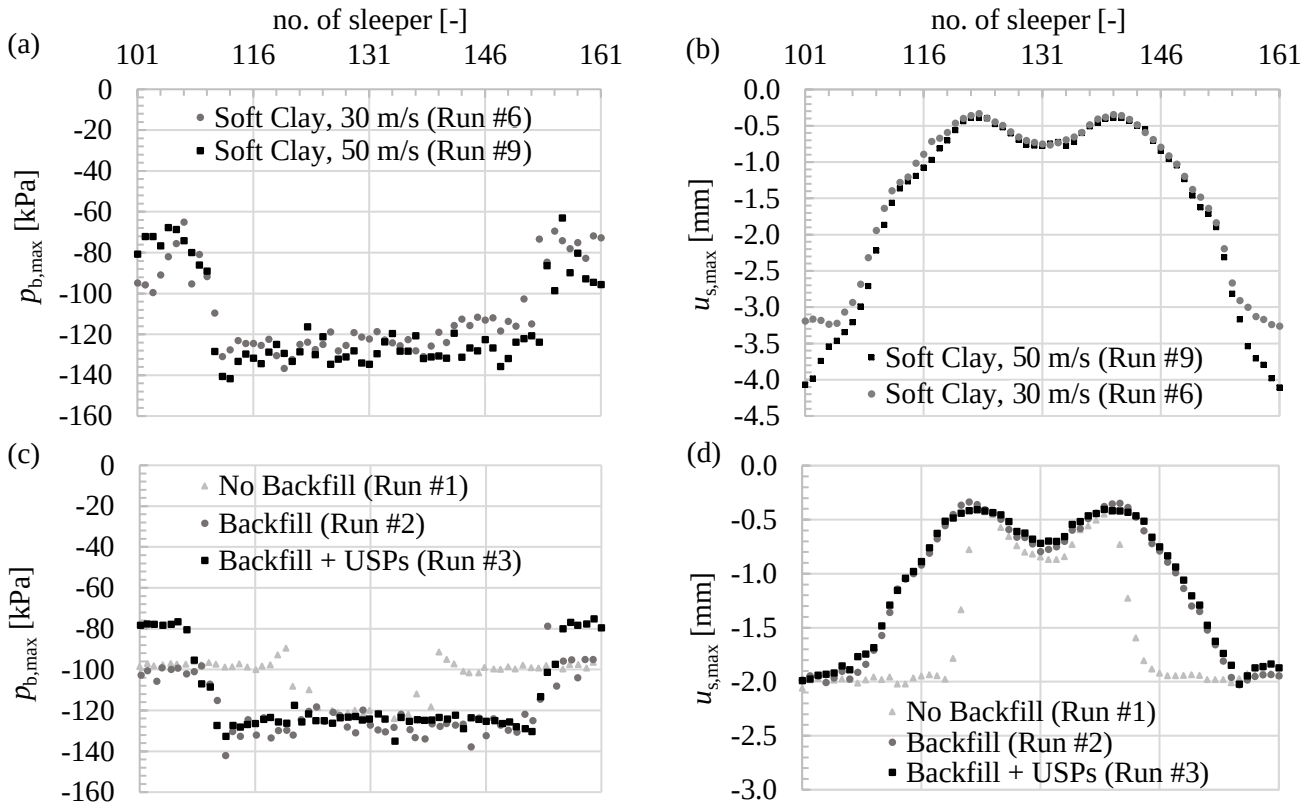

FIGURE 5.2. Calculated maximum sleeper-ballast contact pressure p_{bmax} and maximum sleeper displacement $u_{s,max}$ for (a, b) different train speeds and (c, d) transition solutions.

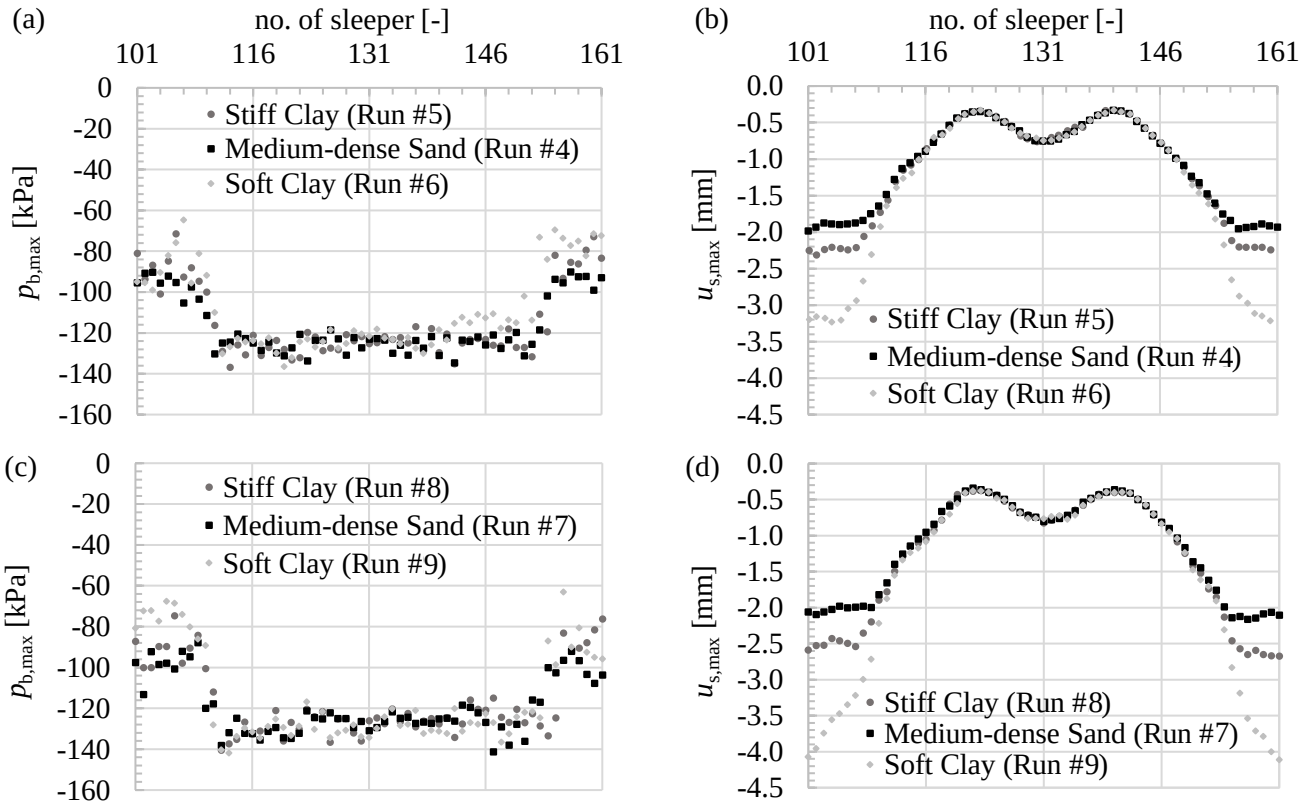

FIGURE 5.3. Calculated max. sleeper-ballast contact pressure p_{bmax} and max. sleeper displacement $u_{s,max}$ for different sub-base materials with train speeds of (a, b) 30 m·s^{-1} and (c, d) 50 m·s^{-1}.

6. ANALYSIS

Short-term simulation results can be used to estimate long-term behaviour using a settlement equation that relates modelling outputs that may vary by sleeper (e.g. load) with settlement and number of cycles. Guérin (1996) suggested that the ballast settlement rate s_N (mm/cycle), at a generic load cycle N, depends on the maximum deflection of the sleeper into the ballast $u_{s,max}$ at that load cycle:

$$s_N = \alpha u_{s,max}^{\beta_g} \tag{6.1}$$

Sato (1997) linked the maximum pressure at the top of ballast immediately below a sleeper $p_{b,max}$ with the settlement rate s_N (mm/10,000 cycles) using two equations. In the second, the ballast settles only if $p_{b,max}$ exceeds a certain threshold p_b^*.

$$s_N = \alpha p_{b,max}^{\beta_s^1} \quad s_N = \alpha\left(p_{b,max} - p_b^*\right)^{\beta_s^2} \tag{6.2}$$

The change in ballast settlement rate using Guérin's equation $i_{s_N}^g$ or Sato's equation $i_{s_N}^s$ under two adjacent sleepers with different load conditions may be computed as:

$$i_{s_N}^g = \frac{s_N\left(u_{s,max}^1\right)}{s_N\left(u_{s,max}^2\right)} = \left(\frac{u_{s,max}^1}{u_{s,max}^2}\right)^{\beta_g} \quad i_{s_N}^s = \frac{s_N\left(p_{b,max}^1\right)}{s_N\left(p_{b,max}^2\right)} = \left(\frac{p_{b,max}^1 - p_b^*}{p_{b,max}^2 - p_b^*}\right)^{\beta_s} \tag{6.3}$$

Using values for the parameters α and β from Grossoni *et al.* (2019) and Li, et al. (2014) (β_g = 1.46; β_s = 5.00), it is possible to estimate the change in ballast settlement rate between adjacent sleepers and hence the development of differential settlement. For example, for two sleepers with maximum downward displacements of 2.0 and 1.5 mm, the ratio of settlement rates will be about 2.1. For two sleepers with maximum sleeper-ballast pressures of 100 and 120 kPa, the ratio of settlement rates will be about 2.5. The simulations were interrogated to determine the maximum values at each sleeper position ($u_{s,max}$, $p_{b,max}$). The sleepers of primary interest were between #100 and #161 (FIGURE 5.1).

The Guérin and Sato equations reflect the importance of maintaining uniform sleeper deflection and sleeper-ballast contact pressures to limit differential settlements between sleepers. Based on the maximum deflections of each sleeper i, $u_{s,max}^i$, three indicators were defined to assess the performance of the transition:

1. the maximum absolute difference between any two adjacent sleepers:

$$I_{max}^{i-j} = max\{|u_{s,max}^{i+1} - u_{s,max}^i|\} \tag{6.4}$$

2. the maximum absolute difference between the bridge and the embankment zones:

$$I_{max}^{e-b} = |\max\{u_{s,max}^i\} - \min\{u_{s,max}^j\}|; \quad i \in S_e, j \in S_b \tag{6.5}$$

   where S_e and S_b are the sets of sleepers on the embankment and bridge respectively.

3. an average rate of change of sleeper displacement with respect to distance along the track in the transition zone:

$$I_{rate}^{tr} = \frac{I_{max}^{e-b}}{l_t} \tag{6.6}$$

   where l_t is the effective length of the transition zone (taken as the distance between the sleepers with the maximum and minimum displacements used in the calculation of I_{max}^{e-b})

These indicators are illustrated in FIGURE 6.1. Equivalent indicators may be developed in terms of the maximum sleeper-ballast pressure.

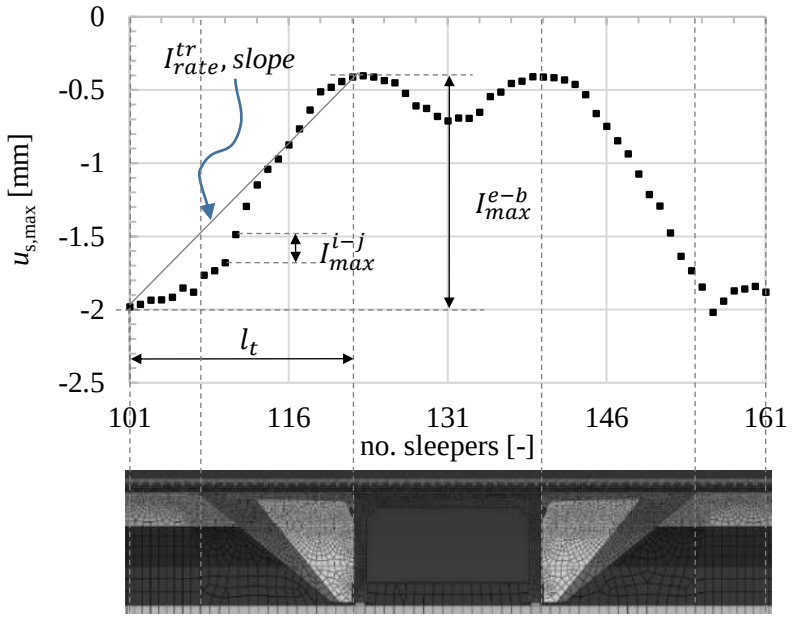

FIGURE 6.1. Graphical representation of the proposed indicators.

TABLE 6.1 summarises the comparative results in terms of the identified indicators. In the table, M.D.S., F.C. and S.C. refer to medium-dense sand, firm clay and soft clay, respectively. The abbreviations B, A and U refer respectively to backfill, approach slab and under sleeper pads.

TABLE 6.1. Final identifies parameters used to compare the different simulation results.

# Run	I^{i-j}_{max}		I^{tr}_{rate}		I^{e-b}_{max}		l_t [no. sleepers]	v_t [m·s^{-1}]	Sub-base	Transition solution
	Value [mm]	Rank [#]	Value [mm/m]	Rank [#]	Value [mm]	Rank [#]				
1	0.37	9	0.61	9	1.63	3	119-123	40	M.D.S.	No solution
2	0.15	3	0.17	3	1.67	5	107-122	40	M.D.S.	B + A
3	0.12	1	0.15	1	1.64	4	105-122	40	M.D.S.	B + A + U
4	0.14	2	0.16	2	1.49	1	108-122	30	M.D.S.	B + A
5	0.16	4	0.19	4	1.87	6	107-122	30	F.C.	B + A
6	0.30	7	0.26	7	2.85	8	105-122	30	S.C.	B + A
7	0.17	5	0.21	5	1.61	2	109-121	50	M.D.S.	B + A
8	0.21	6	0.24	6	2.17	7	107-121	50	F.C.	B + A
9	0.34	8	0.28	8	3.67	9	101-121	50	S.C.	B + A

7. DISCUSSION

Generally, higher speed trains cause increased dynamic wheel-rail interaction loads (Esveld, 2001). The simulations confirm the dynamic amplification effect with increasing speed, which is more significant when the sub-base material is relatively soft. At such conditions, a double detrimental effect is present: an increase in transient sleeper deflections, because of reduced supporting stiffness, and an intensification of dynamic loads resulting from higher train speeds. As the train speed increased from 30 m/s to 50 m/s, the maximum transient vertical sleeper deflection increased by 8.1%, 14.1% and 30.0% for sand, stiff clay, and soft clay, respectively (FIGURE 5.3). Guérin's settlement equation implies that greater transient deflections result in

greater long term settlement; thus the model results suggest that higher train speeds will result in the development of a greater differential permanent settlement between the transition and the bridge.
The peak value of the maximum vertical stress acting on the ballast was only marginally affected by the train speed. In this regard, it is noticeable that the variation of the vertical stress along the bridge section is relatively small for all the simulations (FIGURE 5.3a, 5.3c). However, at the transition points and along the length of the embankment, the maximum vertical stress exhibited noticeable disparities depending on the vehicle speed scenario simulated. This effect was more pronounced for a soft clay subgrade (FIGURE 5.2a).

For the soft clay case, the performance indicators show a substantial increase in I_{max}^{e-b} but the rate of change of displacement, as measured by I_{max}^{i-j} and I_{rate}^{tr}, is not very significant. From FIGURE 5.2b, it can be seen that the effective length of the transition zone, l_t, increases with increased train speed such that rate of change of $u_{s,max}$ remains relatively constant during the transition.

The sub-base material influences the response of the railway track significantly, with a softer material leading to considerably increased maximum sleeper vertical displacements. For a train travelling at 30 m/s, as the earthwork soil changed from sand through stiff to soft clay, the maximum sleeper deflection increased from 1.98 mm to 2.32 mm (+17.2%) and 3.3 mm (+66.7%).

With no transition solution, the variation in maximum sleeper-ballast pressure and sleeper vertical transient displacement is sudden at the bridge abutment (FIGURE 5.2). Following Guerin's and Sato's rules this will potentially increase the permanent differential settlement along the transition between the embankment and the bridge. The presence of a transition solution caused the proposed new indicators to change considerably: I_{max}^{i-j} from 0.37 (no solution) to 0.15 (with backfill solution) and I_{rate}^{tr} from 0.61 to 0.17 (TABLE 6.1). The wedge-shaped backfill and the approach slab mitigate problems by smoothing the change in support stiffness provided to the railway track at least in the idealised scenario analysed.

In recent years there has been growing interest in understanding the benefits of including resilient pads under sleepers (USPs). Lab experiments (e.g. Abadi *et al.*, 2015; Jayasuriya, Indraratna and Ngoc Ngo, 2019), field tests (e.g. Kaewunruen, Aikawa and Remennikov, 2017; Le Pen *et al.*, 2018) and numerical analysis (e.g. Witt, 2008; Wan, Markine and Shevtsov, 2014; Paixão *et al.*, 2018) seem to indicate that USPs can improve track performance by reducing maximum stresses in the trackbed. USPs decrease the effective rail supporting stiffness, causing the wheel loads to be supported by a greater length of the track and reducing the stress acting on the trackbed. Moreover, when USPs are placed at the sleeper to ballast interface, a greater number of contacts between ballast grains and the sleeper is usually experienced, further reducing the grain contact stresses and maximum stresses in the trackbed. However, the properties of USPs (i.e. stiffness, damping, thickness) must be carefully determined depending on the track conditions before installation. Too soft, a USP may excessively increase the maximum vertical rail/sleepers displacements/accelerations. On the contrary, too stiff USPs may not sufficiently influence the effective vertical stiffness of the track, in particular when the track is located on a rigid foundation (e.g. bridge).

Adding USPs to the entire transition zone (FIGURE 4.1b) did not significantly change the track dynamic behaviour. As expected, adding a soft layer between the sleeper and the ballast reduces the contact pressure considerably; along the normal track (FIGURE 5.2), from 100 kPa to 80 kPa (20%). Assuming that the rate

of permanent settlement of the ballast layer is proportional to the maximum vertical stress (Equation 6.3), the permanent differential settlement between the regular track and bridge may increase. If this is true, a better track performance could have been achieved by using USPs only on the bridge deck to decrease the track stiffness. It seems, however, that the sleeper-ballast pressure peak was not significantly reduced on the bridge deck (FIGURE 5.2a). A possible explanation is that the pad used was not soft enough to significantly alter the effective track stiffness. Moreover, no damping was assigned to the USP material. The higher damping of the USPs would minimise the dynamic effect acting on the track.

Among the derived indicators, there is a strong correlation between I_{max}^{i-j} and I_{rate}^{tr} (see ranks in TABLE 6.1), both of which relate to the rate of change of $u_{s,max}$ along the transition zone. These two indicators can be reduced through a stiffness transition solution (e.g. backfill and approach slab). The I_{max}^{e-b} indicator expresses the magnitude of change of $u_{s,max}$ between a normal track and the bridge section and is minimised for the stiffest support (i.e. a medium-dense sand sub-base). The analytical indicators demonstrate that the best performance is achieved for a combination of backfill approach slab track with USPs installed along its length for a medium-dense sand subgrade (see TABLE 6.1), although, as previously mentioned, the benefit of introducing USPs was not substantial for the scenario considered.

CONCLUSIONS

This paper has explored the dynamic behaviour of a bridge transition in the short-term using a 2D FE-model. As a reference, an existing ballasted railway bridge transition was selected; its geometry and material properties were then changed in a parametric study. Three new performance indicators were proposed; these may be formulated in terms of the maximum sleeper deflections or maximum sleeper to ballast contact pressures. They may be used to assess qualitatively the performance of a bridge transition, based on the assumption that differential settlement in the ballast is mainly due to different load conditions at the sleeper / ballast interface.

The effects of train speed, subgrades material and under sleeper pads (USPs) were investigated. Both the train speed and the sub-base material affected the calculated transition performance, in particular with regard to the maximum deflection of the railway track. A stiffer wedge-shaped backfill was found to be adequate to mitigate the adverse effects of the stiffness variation at the bridge approach under idealised conditions.

Adding USPs, all along the transition zone and bridge, did not significantly improve performance. However, no damping was assigned to the USP material, which might have reduced the dynamic effect on the trackbed. The results obtained are highly influenced by the assumed settlement profile of the track. Future work will investigate how initial variations in the track stiffness and geometry will contribute to the development of differential settlement often observed between embankments and bridges.

ACKNOWLEDGMENTS

The authors are grateful for the financial support of the UK Engineering and Physical Sciences Research Council (EPSRC) grant number EP/M025276, and Network Rail.

REFERENCES

Abadi, T. *et al.* (2015) 'Measuring the Area and Number of Ballast Particle Contacts at Sleeper-Ballast and Ballast-Subgrade Interfaces', *International Journal of Railway Technology*, 4(2), pp. 45–72. doi: 10.4203/ijrt.4.2.3.

Abadi, T. *et al.* (2016) 'A Review and Evaluation of Ballast Settlement Models using Results from the Southampton Railway Testing Facility (SRTF)', *Procedia Engineering*. Elsevier B.V., 143, pp. 999–1006. doi: 10.1016/j.proeng.2016.06.089.

Alves Ribeiro, C. (2012) *Transições Aterro - Estrutura em Linhas Ferroviárias de Alta Velocidade: Análise Experimental e Numérica*. University of Porto.

Alves Ribeiro, C. *et al.* (2015) 'Under sleeper pads in transition zones at railway underpasses: numerical modelling and experimental validation', *Structure and Infrastructure Engineering*, 11(11), pp. 1432–1449. doi: 10.1080/15732479.2014.970203.

Arlaud, E. *et al.* (2016) 'Numerical Study of Railway Track Dynamics : The Case of a Transition Zone Dynavoie Method', in *The Third International Conference on Railway Technology: Research, Development and Maintenance*. Cagliari, Italy: Civil-Comp Press, pp. 1–20.

Briaud, J.-L., James, R. W. and Hoffman, S. B. (1997) 'Settlement of Bridge Approaches (The Bump at the End of the Bridge)', *NCHRP Synthesis of Highway Practice*. Transportation Research Board, (234), p. 81.

British Standard Institution (2011) *BS EN 13674-1. Railway applications - Track - Rail Part 1: Vignole railway rails 46 kg/m and above*. UK.

Dahlberg, T. (2001) 'Some railroad settlement models—A critical review', *Proceedings of the Institution of Mechanical Engineers, Part F: Journal of Rail and Rapid Transit*, 215(4), pp. 289–300. doi: 10.1243/0954409011531585.

ERRI (1999) 'Bridge Ends. Embankment Structure Transition: State of the Art Report'. Utrecht, Netherland: European Railway Track.

Esveld, C. (2001) *Modern Railway Track*. Second Edi. Delft, The Netherland: Delft University of Technology.

European Committe for Standardisation (2004) *Eurocode 2: Design of concrete structures - Part 1-1: General rules and rules for buildings*.

Gallego, I. *et al.* (2012) 'Design of embankment–structure transitions for railway infrastructure', *Proceedings of the Institution of Civil Engineers - Transport*, 165(1), pp. 27–37. doi: 10.1680/tran.8.00037.

Gallego, I. *et al.* (2016) 'A mixed slab-ballasted track as a means to improve the behaviour of railway infrastructure', *Proceedings of the Institution of Mechanical Engineers Part F-journal of Rail and Rapid Transit*, 230(7), pp. 1659–1672. doi: 10.1177/0954409715605128.

Getzner Wekstoffe (2019). Available at: http://www.getzner.com.

Grossoni, I. *et al.* (2019) 'The role of track stiffness and its spatial variability on long-term track quality

deterioration', *Proceedings of the Institution of Mechanical Engineers, Part F: Journal of Rail and Rapid Transit*, 233(1), pp. 16–32. doi: 10.1177/0954409718777372.

Guérin, N. (1996) *Approche experimentale et numerique du comportement du ballast des voies ferrees*. Ecole Nationale des Ponts et Chaussées.

Hoppe, E. J. (1999) 'Guidelines for the Use, Design, and Construction of Bridge Approach Slabs', *Virginia Transportation Research Council*, VTRC 00-R4, p. 42.

Jayasuriya, C., Indraratna, B. and Ngoc Ngo, T. (2019) 'Experimental study to examine the role of under sleeper pads for improved performance of ballast under cyclic loading', *Transportation Geotechnics*. Elsevier, 19(October 2018), pp. 61–73. doi: 10.1016/j.trgeo.2019.01.005.

Kaewunruen, S., Aikawa, A. and Remennikov, A. M. (2017) 'Vibration Attenuation at Rail Joints through under Sleeper Pads', *Procedia Engineering*. The Author(s), 189(June), pp. 193–198. doi: 10.1016/j.proeng.2017.05.031.

Li, D. and Davis, D. (2005) 'Transition of Railroad Bridge Approaches', *Journal of Geotechnical and Geoenvironmental Engineering*, 131(11), pp. 1392–1398. doi: 10.1061/(ASCE)1090-0241(2005)131:11(1392).

Li, D., Otter, D. and Carr, G. (2010) 'Railway Bridge Approaches under Heavy Axle Load Traffic: Problems, Causes, and Remedies', *Proceedings of the Institution of Mechanical Engineers, Part F: Journal of Rail and Rapid Transit*, 224(5), pp. 383–390. doi: 10.1243/09544097JRRT345.

Manual of Contract Documents for Highway Works (2016) 'Specification for Highway Works (SHW) - Series 600', p. 132.

Mishra, D. *et al.* (2012) 'Investigation of differential movement at railroad bridge approaches through geotechnical instrumentation', *Journal of Zhejiang University SCIENCE A*, 13(11), pp. 814–824. doi: 10.1631/jzus.A12ISGT7.

Network Rail (2016) *NR/L2/TRK/030. Concrete Sleepes and Bearers*. UK.

Nielsen, J. C. O. and Li, X. (2018) 'Railway track geometry degradation due to differential settlement of ballast/subgrade – Numerical prediction by an iterative procedure', *Journal of Sound and Vibration*. Elsevier Ltd, 412, pp. 441–456. doi: 10.1016/j.jsv.2017.10.005.

Ognibene, G. (2016) *Track Transitions in Railway: Review and Numerical Modelling of a Bridge's Approach*. University of Bologna and University of Southampton.

Paixão, A. *et al.* (2018) 'Numerical simulations to improve the use of under sleeper pads at transition zones to railway bridges', *Engineering Structures*. Elsevier, 164(September 2017), pp. 169–182. doi: 10.1016/j.engstruct.2018.03.005.

Paixão, A., Fortunato, E. and Calçada, R. (2014) 'Transition zones to railway bridges: Track measurements and numerical modelling', *Engineering Structures*, 80, pp. 435–443. doi: 10.1016/j.engstruct.2014.09.024.

Le Pen, L. *et al.* (2018) 'Behaviour of under sleeper pads at switches and crossings – Field measurements', *Proceedings of the Institution of Mechanical Engineers, Part F: Journal of Rail and Rapid Transit*, 232(4), pp. 1049–1063. doi: 10.1177/0954409717707400.

Powrie, W. (2013) *Soil Mechanics: Concepts and Applications*. 3rd edn. CRC Press.

Sañudo, R. *et al.* (2016) 'Track transitions in railways: A review', *Construction and Building Materials*, 112(October), pp. 140–157. doi: 10.1016/j.conbuildmat.2016.02.084.

Sasaoka, C. D. *et al.* (2005) 'Implementing Track Transition Solutions', *Technology Digest TD-05-001*. Pueblo, CO: Transportation Technology Center Inc.

Sato, Y. (1997) 'Optimization of track maintenancework on ballasted track', *In Proceedings of the World Congress on Railway Research (WCRR '97)*, pp. 405–411.

Seo, J. B. (2003) *The Bump at the End of the Bridge: an Investigation*. Texas A&M University.

Shahraki, M. and Witt, K. J. (2015) '3D Modeling of Transition Zone between Ballasted and Ballastless High-Speed Railway Track', *Journal of Traffic and Transportation Engineering*, 3(4), pp. 234–240. doi: 10.17265/2328-2142/2015.04.005.

Stark, T. D. *et al.* (2015) 'Effect of unsupported ties at transition zones', in *Railway Engineering*. Edinburgh, Scotland, p. 13.

Stark, T. D. and Wilk, S. T. (2015) 'Root cause of differential movement at bridge transition zones', *Proceedings of the Institution of Mechanical Engineers, Part F: Journal of Rail and Rapid Transit*, 230(4), pp. 1257–1269. doi: 10.1177/0954409715589620.

Varandas, J. N. (2013) *Long-Term Behaviour of Railway Transitions Under Dynamic Loading*. Nova University of Lisbon.

Varandas, J. N. *et al.* (2014) 'Numerical Modelling of Railway Bridge Approaches: Influence of Soil Non-Linearity', *International Journal of Railway Technology*, 3(4), pp. 73–95. doi: 10.4203/ijrt.3.4.4.

Varandas, J. N., Hölscher, P. and Silva, M. A. (2014) 'Settlement of ballasted track under traffic loading: Application to transition zones', *Proceedings of the Institution of Mechanical Engineers, Part F: Journal of Rail and Rapid Transit*, 228(3), pp. 242–259. doi: 10.1177/0954409712471610.

Wan, C., Markine, V. and Shevtsov, I. (2014) 'Optimisation of the elastic track properties of turnout crossings', *Proceedings of the Institution of Mechanical Engineers, Part F: Journal of Rail and Rapid Transit*, 230(2), pp. 360–373. doi: 10.1177/0954409714542478.

Wang, H. and Markine, V. (2018) 'Modelling of the long-term behaviour of transition zones: Prediction of track settlement', *Engineering Structures*. Elsevier, 156(1), pp. 294–304. doi: 10.1016/j.engstruct.2017.11.038.

White, W., Lee, I. K. and Valliappan, S. (1977) 'Unified boundary for finite dynamic models', *Journal of the Engineering Mechanics Division*, 103, pp. 949–964.

Wilk, S. T. and Stark, T. D. (2016) 'Modeling Progressive Settlement of a Railway Bridge Transition', (June). doi: 10.1115/JRC2016-5715.

Witt, S. (2008) *The Influence of Under Sleeper Pads on Railway Track Dynamics, Engineering*. University of Linköping.

Zuada Coelho, B. E. (2011) *Dynamics of railway transition zones in soft soils*. University of Porto.